

# Halo model prediction of the cosmic magnification statistics: the full non-linear contribution

Masahiro Takada<sup>1</sup>\* and Takashi Hamana<sup>2,3†</sup>

<sup>1</sup> Department of Physics and Astronomy, University of Pennsylvania, 209 S. 33rd Street, Philadelphia, PA 19104, USA

<sup>2</sup> Institut d’Astrophysique de Paris, 98 bis Bld Arago, F-75014, Paris, France

<sup>3</sup> National Astronomical Observatory of Japan, Mitaka, Tokyo 181-8588, Japan

arXiv:astro-ph/0305381v1 20 May 2003

19 June 2019

## ABSTRACT

We use the halo model formulation of Takada & Jain (2003) to compute the correlation function of lensing magnification due to the large-scale structure. We do not employ the weak lensing approximation,  $\mu \approx 1 + 2\kappa$ , and our predictions thus include the full contribution from non-linear magnification,  $\mu \gtrsim 2$ , due to lensing halos. We compare the model prediction with ray-tracing simulations and find excellent agreement over a range of angular scales we consider ( $0'.5 \lesssim \theta \lesssim 30'$ ). In addition, the asymptotic behavior for large magnifications is derived based on the universal properties of magnification around caustic curves, in analogy with the asymptotic scaling of the probability distribution function;  $\text{PDF}(\mu) \propto \mu^{-3}$ . For a general correlation function parameterized as  $\langle \mu^p f \rangle$  ( $f$  is any cosmic field correlated with the magnification field), the amplitude is finite for  $p < 1$  and diverges for  $p \geq 1$  as  $\mu \rightarrow \infty$ , independent of details of the lensing mass distribution and the separation angle. This consequence is verified by the halo model as well as by the simulations.

We find that the non-linear magnification contribution significantly enhances the amplitude of the magnification correlation, e.g. by  $\gtrsim 50\%$  on scales  $\lesssim 3'$ , relative to the weak lensing prediction. Further, it is shown that the non-linear effect remains even on large scales  $\gtrsim 10'$ , where it is naively expected that the weak lensing approximation is safely valid. The non-linear effect is more significant for sources at higher redshifts. Therefore, it is important to account for the non-linear contribution in theoretical models in order to make a correct interpretation of measurements expected from forthcoming massive surveys. It is demonstrated that the magnification correlation displays stronger sensitivity to density profiles of halos with  $M \geq 10^{13} M_\odot$  than cosmic shear statistics. This implies that joint measurements can be used to put stringent constraints on structure formation models.

**Key words:** cosmology: theory — gravitational lensing — large-scale structure of universe

## 1 INTRODUCTION

Gravitational lensing caused by the large-scale structure is now recognized as a powerful cosmological tool (Mellier 1999; Bartelmann & Schneider 2001 for thorough reviews). The gravitational deflection of light causes an increase or decrease of the area of a given patch on the sky depending on which the light ray passes preferentially through the overdense or underdense region. Accordingly, this causes an observed image of source to be magnified or demagnified relative to the unlensed image, since lensing conserves the surface brightness and the received luminosity is proportional to the solid angle of the image. Large magnifications are observed in a strong lensing system with the clear signature of multiple images

or largely deformed images. It has been also proposed that modest magnification is measurable in a statistical sense. The magnification leads to an enhancement in the flux-limited number count of background sources around foreground sample that traces the lensing mass distribution. Based on this idea, numerous works have investigated the QSO-galaxy cross correlation theoretically (e.g., Broadhurst, Taylor & Peacock 1995; Bartelmann 1995) as well as observationally (e.g., Benítez & Martínez-González 1997; Benítez et al. 2001; Gaztañaga 2002; also see Bartelmann & Schneider 2001 for a thorough review). Further, Jain (2002) recently proposed that the magnification effect can be extracted by statistically dealing with size fluctuations of distant galaxy images, though it is a great challenging for existing data yet. Forthcoming massive

\* E-mail: mtakada@hep.upenn.edu

† E-mail: hamana@iap.fr

surveys such as SDSS<sup>1</sup>, DLS<sup>2</sup>, the CFHT Legacy survey<sup>3</sup> as well as future precise imaging surveys such as SNAP<sup>4</sup>, Pan-STARRS<sup>5</sup> and LSST<sup>6</sup> promise measurements of these magnification effects. Therefore, it is of great importance to explore how this type of method can be a useful cosmological tool and how complementary to the established cosmic shear method, which measures correlation between lensing induced ellipticities of distant galaxy images (e.g., Hamana et al. 2002 and Jarvis et al. 2003 and references therein).

The magnification field  $\mu(\theta)$  in a given direction  $\theta$  on the sky is expressed (e.g., Schneider, Falco & Ehlers 1992) as

$$\mu(\theta) = |(1 - \kappa(\theta))^2 - \gamma^2(\theta)|^{-1}. \quad (1)$$

Here  $\kappa$  and  $\gamma$  are the convergence and shear fields, which are fully determined by the intervening mass distribution. This equation means that the magnification becomes non-linear ( $\mu \gtrsim 2$ ) or even formally infinite when the lensing fields  $\kappa, \gamma \sim O(1)$ . This happens when the light ray emitted from a source encounters an intervening mass concentration, i.e., dark matter halo such as galaxy or cluster of galaxies. It is known that strong lensing of  $\mu \gg 2$  can be used to probe detailed mass distribution within a halo (e.g., Hattori et al. 1999). Similarly, modest non-linear magnifications of  $\mu \gtrsim 2$  could lead to a sensitivity of the magnification statistics to the halo structure in a statistical sense, as investigated in this paper. A fundamental result of cold dark matter (CDM) model simulations is that the density profiles of halos are universal across a wide range of mass scales (e.g., Navarro, Frenk & White 1997, hereafter NFW). On the other hand, some alternative models such as self-interacting dark matter scenario (Spergel & Steinhardt 2000) have been proposed in order to reconcile the possible conflicts between the simulation prediction and the observation on halo scales. If dark matter particle has a non-negligible self-interaction between themselves, the effect is likely to yield a drastic change on the halo profile from the CDM model prediction (Yoshida et al. 2000). The halo structure thus reflects the dark matter nature as well as detailed history of non-linear gravitational clustering. Hence, exploring the halo profile properties with gravitational lensing can be a direct test of the CDM paradigm on scales  $\lesssim$  Mpc, which is not attainable with the cosmic microwave background measurement.

The simplest statistical quantity most widely used in cosmology is the two-point correlation function (2PCF). For our purpose, the magnification field is taken as either or both of the two fields entering into the correlation function. However, it is not straightforward to analytically compute the magnification 2PCF because of the non-linear relation between  $\mu$  and  $\kappa, \gamma$ , where the latter fields are easier to compute in a statistical sense based on a model of the mass power spectrum. For this reason, the conventional method of the magnification statistics employs the weak lensing approximation  $\mu \approx 1 + 2\kappa$  (e.g., Bartelmann 1995; Dolag & Bartelmann 1997; Sanz et al. 1997; Benitez & Martínez-González 1997; Moessner & Jain 1998; Benitez et al. 2001; Ménard & Bartelmann 2002; Gaztañaga et al. 2002; Jain et al. 2003). However, it is obvious that this type of method is valid only in the limit  $\kappa, \gamma \ll 1$  and likely degrades the model accuracy on non-linear small scales. In fact, using the ray-tracing simulations Ménard et al. (2002) clarified the

significant importance of the non-linear magnification contribution to the magnification statistics (see also Barber & Taylor 2003). It was shown that the perturbative treatment breaks down over a range of angular scales of our interest. Although an alternative promising method is to employ ray-tracing simulations, to perform multiple evaluations in model parameter space requires sufficient number of simulation runs, which is relatively prohibitive.

Therefore, the purpose of this paper is to develop an analytic method to compute the magnification induced correlation function without employing the weak lensing approximation. To do this, we use the halo model to describe gravitational clustering in the large-scale structure, following the method developed in Takada & Jain (2003a,b,c, hereafter TJ03a,b,c). The encouraging results revealed in the literature are that, even though the halo model rather relies on the simplified assumptions, it has led to consistent predictions to interpret observational results of galaxy clustering as well as to reproduce simulation results (e.g., see Seljak 2000; Zehavi et al. 2003; Takada & Jain 2002, hereafter TJ02; TJ03a,b,c; also see Cooray & Sheth 2002 for a review).

The plan of this paper is as follows. §2 presents the basic equations relevant for cosmological gravitational lensing and then briefly summarize two promising methods to statistically measure the magnification effect. In §3 we develop an analytic method to compute the magnification correlation functions based on the halo model. In §4, we derive an asymptotic behavior of the correlation amplitude for large magnifications. In §5 we qualitatively test the halo model prediction and the asymptotic behavior using ray-tracing simulations. §6 is devoted to a summary and discussion. Throughout this paper, without being explicitly stated, we consider the  $\Lambda$ CDM model with  $\Omega_{m0} = 0.3$ ,  $\Omega_{\lambda0} = 0.7$ ,  $\Omega_{b0} = 0.0227$ ,  $h = 0.7$  and  $\sigma_8 = 0.9$ . Here  $\Omega_{m0}$ ,  $\Omega_{b0}$  and  $\Omega_{\lambda0}$  are the present-day density parameters of matter, baryons and the cosmological constant,  $h$  is the Hubble parameter, and  $\sigma_8$  is the rms mass fluctuation in a sphere of radius  $8h^{-1}$ Mpc.

## 2 PRELIMINARIES

### 2.1 Magnification of gravitational lens

The gravitational deflection of light ray induces a mapping between the two-dimensional source plane (S) and the image plane (I) (e.g., Schneider, Ehlers & Falco 1992):

$$\delta\theta_i^S = \mathcal{A}_{ij} \delta\theta_j^I, \quad (2)$$

where  $\delta\theta_i$  is the separation vector between points on the respective planes. The lensing distortion of an image is described by the Jacobian matrix  $\mathcal{A}_{ij}$  defined as

$$\mathcal{A} = \begin{pmatrix} 1 - \kappa - \gamma_1 & -\gamma_2 \\ -\gamma_2 & 1 - \kappa + \gamma_1 \end{pmatrix}, \quad (3)$$

where  $\kappa$  is the lensing convergence and  $\gamma_1$  and  $\gamma_2$  denote the tidal shear fields, which correspond to elongation or compression along or at  $45^\circ$  to  $x$ -axis, respectively, in the given Cartesian coordinate on the sky. The  $\kappa$  and  $\gamma_i$  depend on angular position, although we have omitted showing it in the argument for simplicity. Since the gravitational lensing conserves surface brightness from a source, the lensing magnification, the ratio of the fluxes observed from the image to that from the unlensed source, is given by determination of the deformation matrix, yielding equation (1). In the weak lensing limit  $\kappa, \gamma \ll 1$ , one could Taylor expand the magnification field as  $\mu \approx 1 + 2\kappa$ , as conventionally employed in the literature to compute the magnification statistics.

<sup>1</sup> <http://www.sdss.org/>

<sup>2</sup> [dls.bell-labs.com/](http://dls.bell-labs.com/)

<sup>3</sup> [www.cfht.hawaii.edu/Science/CFHLS/](http://www.cfht.hawaii.edu/Science/CFHLS/)

<sup>4</sup> [snap.lbl.gov](http://snap.lbl.gov)

<sup>5</sup> [www.ifa.hawaii.edu/pan-starrs/](http://www.ifa.hawaii.edu/pan-starrs/)

<sup>6</sup> [www.dmtlescope.org/dark\\_home.html](http://dmtlescope.org/dark_home.html)

In the context of cosmological gravitational lensing, the convergence field is expressed as a weighted projection of the three-dimensional density fluctuation field between source and observer:

$$\kappa(\boldsymbol{\theta}) = \int_0^{\chi_H} d\chi W(\chi) \delta[\chi, d_A(\chi) \boldsymbol{\theta}], \quad (4)$$

where  $\chi$  is the comoving distance,  $d_A(\chi)$  is the comoving angular diameter distance to  $\chi$ , and  $\chi_H$  is the distance to the Hubble horizon. Note that  $\chi$  is related to redshift  $z$  via the relation  $d\chi = dz/H(z)$  ( $H(z)$  is the Hubble parameter at epoch  $z$ ). Following the pioneering work done by Blandford et al. (1991), Miralda-Escude (1991) and Kaiser (1992), we used the Born approximation, where the convergence field is computed along the unperturbed path, neglecting higher order terms that arise from coupling between two or more lenses at different redshifts. Using ray-tracing simulations of the lensing fields, Jain et al. (2000) proved that the Born approximation is a good approximation for lensing statistics (see also Van Waerbeke et al. 2001; Vale & White 2003). The lensing weight function  $W$  is given by

$$W(\chi) = \frac{3}{2} \Omega_{m0} H_0^2 a^{-1}(\chi) d_A(\chi) \times \int_{\chi}^{\chi_H} d\chi_s f_s(\chi_s) \frac{d_A(\chi_s - \chi)}{d_A(\chi_s)}, \quad (5)$$

where  $f_s(\chi_s)$  is the redshift selection function normalized as  $\int_0^{\chi_H} d\chi f_s(\chi) = 1$ . In this paper we assume all sources are at a single redshift  $z_s$  for simplicity;  $f_s(\chi) = \delta_D(\chi - \chi_s)$ .  $H_0$  is the Hubble constant ( $H_0 = 100h \text{ km s}^{-1} \text{Mpc}^{-1}$ ). Similarly, the shear fields are derivable from the density fluctuation fields, but the relation is non-local due to the nature of the gravitational tidal force. In Fourier space, we have the simple relation between  $\kappa$  and  $\gamma$ :

$$\tilde{\gamma}_1(\boldsymbol{l}) = \cos 2\varphi_{\boldsymbol{l}} \tilde{\kappa}(\boldsymbol{l}), \quad \tilde{\gamma}_2(\boldsymbol{l}) = \sin 2\varphi_{\boldsymbol{l}} \tilde{\kappa}(\boldsymbol{l}), \quad (6)$$

where the Fourier-mode vector is  $\boldsymbol{l} = l(\cos \varphi_{\boldsymbol{l}}, \sin \varphi_{\boldsymbol{l}})$ .

## 2.2 Methodology for measuring the magnification statistics

There are two promising ways for measuring the lensing magnification effect statistically, which are likely feasible for forthcoming and future surveys. Here we briefly summarize the methodology.

Gravitational magnification has two effects. First, it causes the area of a given patch on the sky to increase, thus tending to dilute the number density. Second, sources fainter than the limiting magnitude are brightened and may be included in the sample. The net effect, known as the magnification bias, depends on how the loss of sources due to dilution is balanced by the gain of sources due to flux magnification. Therefore, it depends on the slope  $s$  of the unlensed number counts of sources  $N_0(m)$  in a sample with limiting magnitude  $m$ ,  $s = d \log N_0(m) / dm$ . Magnification by amount  $\mu$  changes the number counts to (e.g., Broadhurst, Taylor & Peacock 1995; Bartelmann 1995):

$$N'(m) = N_0(m) \mu^{2.5s-1}. \quad (7)$$

For the critical value  $s = 0.4$ , magnification does not change the number density; it leads to an excess for  $s > 0.4$ , and a deficit for  $s < 0.4$ . Let  $n_1(\boldsymbol{\theta})$  be the number density of foreground sample with mean redshift  $\langle z \rangle_1$ , observed in the direction  $\boldsymbol{\theta}$  on the sky, and  $n_2(\boldsymbol{\theta})$  that of the source sample with a higher mean redshift  $\langle z \rangle_2 > \langle z \rangle_1$ . Thus, even if there is no intrinsic correlation between the two populations, magnification induces the non-

vanishing cross-correlation:

$$\begin{aligned} \xi(\boldsymbol{\theta}) &= \langle \delta n_1(\boldsymbol{\theta}_1) \delta n_2(\boldsymbol{\theta}_2) \rangle_{|\boldsymbol{\theta}_1 - \boldsymbol{\theta}_2| = \theta} \\ &= \langle \delta n_1(\boldsymbol{\theta}_2) [\mu(\boldsymbol{\theta}_2)]^{2.5s-1} \rangle_{|\boldsymbol{\theta}_1 - \boldsymbol{\theta}_2| = \theta}, \end{aligned} \quad (8)$$

where  $\delta n_i(\boldsymbol{\theta}) = (n_i(\boldsymbol{\theta}) - \bar{n}_i)/\bar{n}_i$ , with  $\bar{n}_i$  the average number density of the  $i$ th sample. Here  $\langle \dots \rangle$  denotes the ensemble average and observationally means the average over all pairs separated by  $\theta$  on the sky. Based on this idea, numerous studies have confirmed the existence of the enhancement of the QSO number counts around foreground galaxies, i.e., QSO-galaxy cross correlation (e.g., Benítez et al. 2001, Gaztañaga 2002 and references therein; also see Bartelmann & Schneider 2001 for a review). Although these results are in qualitatively agreement with the magnification bias, in most cases the amplitude of the correlation is much higher than that expected from gravitational lensing models. The excess might be due to the non-linear magnification contribution from massive halos. However, to make such a statement with confidence, it is necessary to further explore an obstacle in the theoretical model, the bias relation between the galaxy and mass distributions. This still remains uncertain observationally and theoretically. In particular, on small scales ( $\lesssim \text{Mpc}$ ), it is crucial to model how to populate halos of given mass with galaxies, known as the halo occupation number (e.g., Seljak 2000; TJ03b). Recently, Jain, Scranton & Sheth (2003) carefully examined the effect of the halo occupation number on the magnification bias and showed that these parameters yield a strong sensitivity to the predicted correlation. For example, possible modification for types of galaxies leads to a change of a factor of 2-10 in the expected signal on arcminute scales.

Second, Jain (2002) recently proposed a new method for measuring the magnification effect of the large-scale structure, based on the work of Bartelmann & Narayan (1995). The lensing effect is to increase or decrease an observed image of galaxy relative to the unlensed image, depending on which the light ray travels preferentially through overdense or underdense region that corresponds to  $\mu > 1$  or  $\mu < 1$ . That is, the area  $S$  and characteristic radius  $R(\propto S^{1/2})$  are changed by the magnification field  $\mu$  as

$$S \rightarrow S\mu, \quad R \rightarrow R\mu^{1/2}. \quad (9)$$

Although the unlensed image is not observable, this effect can be statistically extracted as follows. We can first estimate the mean size of source galaxies from the average over a sufficient number of sample, under the assumption  $\langle \mu \rangle = 1$  or  $\langle \mu^{1/2} \rangle = 1$ , which will be a good approximation in a realistic inhomogeneous universe (e.g., Weinberg 1978). Then, the two-point correlation function (2PCF) of the size fluctuations can be computed from the average over all pairs of galaxies separated by the angle considered, in analogy with the 2PCF of the cosmic shear fields (the variance method was considered in Jain 2002). The reason that this method is not yet feasible is that it requires a well controlled estimate of the unlensed size distribution as well as systematics (photometric calibration, resolution for sizes and psf anisotropy). Hence, space based imaging surveys will make possible the measurement of galaxy sizes with a sufficient accuracy hard to achieve from the ground so far. This method can potentially be a precise cosmological probe like the cosmic shear measurement, because it is free of the galaxy bias uncertainty. Further, the non-linear nature of the magnification could lead to complementarity to the cosmic shear measurement, as we will discuss below.

### 3 HALO APPROACH TO MAGNIFICATION STATISTICS

#### 3.1 Halo profile and mass function

We use the halo model of gravitational clustering to compute the magnification statistics, following the method in TJ03a,b,c. Key model ingredients are the halo profile  $\rho_h(r)$ , the mass function  $n(M)$ , and the halo bias  $b(M)$ , each of which is well investigated in the literature.

As for the halo profile, we employ an NFW profile truncated at radius  $r_{180}$ , which is defined so that the mean density enclosed by sphere with  $r_{180}$  is 180 times the background density. Within a framework of the halo model, we need to express the NFW profile in terms of  $M_{180}$  and redshift  $z$ . To do this, we first express the two parameters of the NFW profile, the central density parameter and the scale radius, in terms of the virial mass and redshift, based on the spherical top-hat collapse model and the halo concentration parameter of Bullock et al. (2001) (see TJ03b,c for more details). Then, following Hu & Kravtsov (2002), we employ a conversion method between the virial mass and  $M_{180}$  in order to re-express the NFW profile in terms of  $M_{180}$  and  $z$ . In what follows, we will often refer halo massed  $M$  as  $M_{180}$  for simplicity.

For the mass function, we employ the Sheth-Tormen mass function (Sheth & Tormen 1999):

$$\begin{aligned} n(M)dM &= \frac{\bar{\rho}_0}{M} f(\nu)d\nu \\ &= \frac{\bar{\rho}_0}{M} A[1 + (a\nu)^{-p}]\sqrt{a\nu} \exp\left(-\frac{a\nu}{2}\right) \frac{d\nu}{\nu}, \end{aligned} \quad (10)$$

where  $\nu$  is the peak height defined by

$$\nu = \left[ \frac{\delta_c(z)}{D(z)\sigma(M)} \right]^2. \quad (11)$$

Here  $\sigma(M)$  is the present-day rms fluctuation in the mass density, smoothed with a top-hat filter of radius  $R_M \equiv (3M/4\pi\bar{\rho}_0)^{1/3}$ ,  $\delta_c$  is the threshold overdensity for the spherical collapse model and  $D(z)$  is the linear growth factor (e.g., Peebles 1980). The numerical coefficients  $a$  and  $p$  are taken from the results of Table 2 in White (2002) as  $a = 0.67$  and  $p = 0.3$ , which are different from the original values  $a = 0.707$  and  $p = 0.3$  in Sheth & Tormen (1999). Note that the normalization coefficient  $A = 0.129$ . The main reason we employ the halo boundary  $r_{180}$  is that the mass function measured in  $N$ -body simulations can be better fitted by the universal form (10) when one employs the halo mass estimator of  $M_{180}$ , than using the virial mass estimator, as carefully examined in White (2002). To maintain the consistency, we also employ the halo biasing  $b(M)$  given in Sheth & Tormen (1999) with the same  $a$  and  $p$  parameters, which is needed for the 2-halo term calculation. Note that  $\int dM b(M)n(M)M/\bar{\rho}_0 \simeq 1$  for the halo bias model and the mass function we employ (e.g., Seljak 2000).

#### 3.2 Lensing fields for an NFW profile

For an NFW profile, we can derive analytic expressions to give the radial profiles of convergence, shear and magnification.

For a given source at redshift  $z_s$ , the convergence profile for a halo of mass  $M$  at  $z$ , denoted by  $\kappa_M$ , can be given as a function of the projected radius from the halo center:

$$\kappa_M(\theta) = 4\pi G a^{-1} \frac{d_A(\chi)d_A(\chi_s - \chi)}{d_A(\chi_s)} \frac{Mf}{2\pi r_s^2} F(\theta/\theta_s), \quad (12)$$

where  $r_s$  is the scale radius and  $\theta_s$  its projected angular scale. The

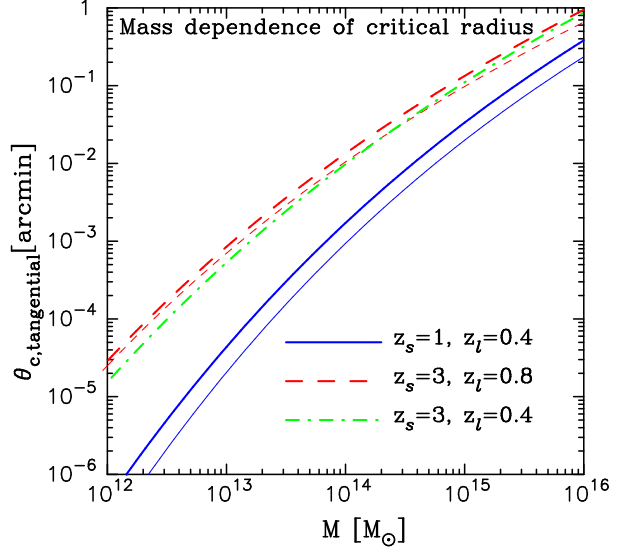


**Figure 1.** The tangential critical radius of NFW profile against halo masses. The solid and dashed curves are the results for lensing halos at redshifts of  $z_l = 0.4$  and  $0.8$  for source redshifts of  $z_s = 1$  and  $z_s = 3$ , respectively. Even if we consider a lower lens redshift, the result does not largely change, as shown by the dot-dashed curve. The respective thin curves are the results when we ignore the shear contribution to the magnification field.

explicit form of  $F(x)$  is given by equation (27) in TJ03b. For an axially symmetric profile, the shear amplitude can be derived as

$$\begin{aligned} \gamma_M(\theta) &= \bar{\kappa}(\theta) - \kappa(\theta) \\ &= 4\pi G a^{-1} \frac{d_A(\chi)d_A(\chi_s - \chi)}{d_A(\chi_s)} \frac{Mf}{2\pi r_s^2} G(\theta/\theta_s), \end{aligned} \quad (13)$$

where  $G(x)$  is given by equation (16) in TJ03c. These expressions of  $\kappa_M$  and  $\gamma_M$  differ from those given in Bartelmann (1996), which are derived from an *infinite* line-of-size projection of the NFW profile under the implicit assumption that the profile is valid (even far) beyond the virial radius. TJ03b,c carefully verified that employing the expressions (12) and (13) in the real-space halo model is essential to achieve the model accuracy as well as the consistency with the Fourier-space halo model well investigated in the literature (e.g., Seljak 2000).

Throughout this paper we employ the halo boundary  $r_{180}$ , not the virial radius, as stated in §3.1. For this setting, we have to replace parameter  $c$  used in  $F(x)$  and  $G(x)$  in TJ03b,c with the ratio of the scale radius to  $r_{180}$ ,  $c_{180}$ . The relation between  $c_{180}$  and  $c$  is given by  $c_{180} = cr_{180}/r_{\text{vir}}$ . Note that, even if we use the virial boundary, the results shown in this paper are almost unchanged.

Given the convergence and shear profiles for a halo of mass  $M$ , the magnification field is given by  $\mu_M(\theta) = |(1 - \kappa_M(\theta))^2 - \gamma_M^2(\theta)|^{-1}$ . This equation implies that  $\mu_M$  could be formally infinity at some critical radius when the denominator becomes zero. The radius in the lens plane is called the critical curve, while the corresponding curve in the source plane is the caustic curve.

Any lensing NFW halo inevitably provides *finite* critical radius. This is because the convergence  $\kappa_M$  varies from zero to infinity with changing radius from  $\theta_{180}$  to 0, while the shear remains finite over the range (see Figure 2 in TJ03c). Figure 1 plots the tangential critical radius for a lensing NFW halo against the mass. Note that an NFW profile produces two critical radii – an outer curve causes a tangentially deformed image around it, while the

inner one causes a radially deformed image. The solid and dashed curves are the results for halos at redshifts  $z_l = 0.4$  and  $0.8$  for source redshifts of  $z_s = 1.0$  and  $3.0$ , respectively. One can see that the critical radius has a strong dependence on halo masses and is larger for  $z_s = 3$  than for  $z_s = 1$  due to the greater lensing efficiency. These critical curves do not largely change even if we consider a lower lens redshift than the peak redshift, as shown by the dot-dashed curve. Massive halos with  $M \geq 10^{15} M_\odot$  provide the critical radii of  $\gtrsim 0.1'$ . However, this does not mean that the non-linear effect on the magnification correlation functions appears only on scales  $\lesssim 1'$ . Rather, the important implication revealed here is that large magnification events with  $\mu \gg 2$  have a finite cross section to the correlation evaluation. Modest non-linear magnifications ( $\mu \gtrsim 2$ ) have the greater cross section. Finally, the respective thin curves are the results if we ignore the shear contribution to the magnification (1), which manifests the importance of the shear contribution.

### 3.3 Real-space halo model approach

In this subsection, we present the halo model method to compute the magnification induced correlation function. First, we simply consider the 2PCF defined as

$$\xi_\mu(\theta) \equiv \langle [\mu(\phi) - 1][\mu(\phi + \theta) - 1] \rangle, \quad (14)$$

where  $\mu - 1$  is the magnification fluctuation field. This 2PCF is observable from area fluctuations of distant galaxy images, as discussed in §2.2.

From a picture of the halo model,  $\xi_\mu(\theta)$  can be expressed as sum of correlations between the magnifications fields within a single halo (1-halo term) and between two different halos (2-halo term):

$$\xi_\mu(\theta) = \xi_\mu^{1h}(\theta) + \xi_\mu^{2h}(\theta). \quad (15)$$

It is straightforward to extend the real-space halo model developed in TJ03a,b,c to compute the 1-halo term contribution, which has dominant contribution on small non-linear scales (see equations (19) and (20) in TJ03c):

$$\begin{aligned} \xi_\mu^{1h}(\theta) &= \int_0^{\chi_H} d\chi \frac{d^2V}{d\chi d\Omega} \int dM n(M) \\ &\times \int_0^\infty d\phi \int_0^{2\pi} d\varphi \phi [\mu_M(\phi) - 1] [\mu_M(|\phi + \theta|) - 1], \end{aligned} \quad (16)$$

where we have introduced the polar coordinate  $d^2\phi = \phi d\phi d\varphi$ ,  $d^2V/d\chi d\Omega = d_A^2(\chi)$  for a flat universe and we can set the separation vector  $\theta$  to be along the first axis from statistical symmetry, thereby  $|\phi + \theta| = (\phi^2 + \theta^2 + 2\phi\theta \cos\varphi)^{1/2}$ . We have assumed a uniform distribution of sources on the sky and ignored a probability of multiple images and an increase or decrease in sampling of the images due to the lensing itself. The equation above implies that the 1-halo term contribution is given by summing lensing contributions due to halos along the line-of-sight weighted with the halo number density on the light cone. Note that the integration range of  $d^2\phi$  is taken as the infinite area, taking into account the non-local property of the shear field that is non-vanishing at radius outside the halo boundary. In practice, setting the upper bound of  $\int d\phi$  to be three times the projected radius  $\theta_{180}$  gives the same result, to within a few percents. The validity of the real-space halo model formulation was carefully investigated in TJ03b,c.

As discussed in §3.2 and shown in Figure 1, an NFW profile always provides finite critical curves, where the magnification

formally becomes infinity. Therefore, to make the halo model prediction, we introduce a magnification cutoff  $\mu_{\max}$  in the calculation – the integration range of  $\int d^2\phi$  is confined to the region satisfying the condition  $\mu_M \leq \mu_{\max}$  for each halo. This procedure is somehow similar to what is done in the measurement from ray-tracing simulations, where a masking of high magnification events is employed to avoid a significant statistical scatter (e.g., see Ménard et al. 2002; Barber & Taylor 2002). Thus the halo model to some extent allows for a fair comparison of the prediction with the simulation result, which is not attainable by the perturbative treatment. However, note that the procedure taken in the halo model ignores the lensing projection effect for simplicity: exactly speaking, the maximum magnification should be given by the lensing fields between source and observer, not by those of individual halo.

Next, we consider the 2-halo term contribution to  $\xi_\mu$ . Similarly, based on the real-space halo model, the 2-halo term can be expressed as

$$\begin{aligned} \xi_\mu^{2h}(\theta) &= \int_0^\infty d\chi \frac{d^2V}{d\chi d\Omega} \int dM n(M) \int dM' n(M') \\ &\times \int d^2\phi [\mu_M(\phi) - 1] \int d^2\phi' [\mu_{M'}(\phi') - 1] \\ &\times b(M)b(M') \int \frac{l dl}{2\pi} P^L \left( k = \frac{l}{d_A}; \chi \right) J_0(l|\theta - \phi - \phi'|), \end{aligned} \quad (17)$$

where  $J_0(x)$  is the zero-th order Bessel function and  $P^L(k)$  is the linear mass power spectrum at epoch  $\chi$  as given by  $P^L(k; \chi) = D^2(\chi)P(k; t_0)$ . The term including  $P^L(k)$  in the third line on the r.h.s denotes the angular two-point function between different halos of masses  $M$  and  $M'$ , which is derived using Limber's equation and the flat-sky approximation (e.g., Blandford et al. 1991; Miralda-Escude 1991; Kaiser 1992). We similarly introduce the maximum magnification cutoff in the 2-halo term calculation as in the 1-halo term. The equation above means that we have to perform an 8-dimensional integration to get the 2-halo term, which is computationally intractable. For this reason, we employ an approximated way to be valid when angular separation between the two halos taken on the sky is greater than the separation angle  $\theta$ :  $\theta \gg \phi, \phi'$ . This leads to simplified expression of the 2-halo term:

$$\begin{aligned} \xi_\mu^{2h}(\theta) &\approx \int_0^\infty d\chi \frac{d^2V}{d\chi d\Omega} \\ &\times \left[ \int dM b(M) n(M) \int \phi d\phi 2\pi (\mu_M(\phi) - 1) \right]^2 \\ &\times \int \frac{l dl}{2\pi} P^L \left( k = \frac{l}{d_A(\chi)}; \chi \right) J_0(l\theta). \end{aligned} \quad (18)$$

This allows us to get the 2-halo term by a three-dimensional integration, because the integrations of the second and third lines on the r.h.s can be done separately before performing the  $\chi$ -integration. It is worth checking the consistency of the 2-halo term above with the limiting case  $\xi_\mu \approx 4\xi_\kappa$ , which is valid only in the weak lensing approximation  $\mu \approx 1 + 2\kappa$  for  $\kappa, \gamma \ll 1$ . In this limit, the term contained in the second line on the r.h.s of equation (18) can be rewritten as

$$\begin{aligned} &\int dM b(M) n(M) \int d^2\phi (\mu_M(\phi) - 1) \\ &\approx \int dM b(M) n(M) \int d^2\phi 2\kappa_M(\phi) \end{aligned}$$

$$= 2W(\chi)d_A^{-2}(\chi) \int dM b(M)n(M) \frac{M}{\rho_0}, \quad (19)$$

where the second equality is derived from equations (25) and (28) in TJ03b. Therefore, substituting this result into the 2-halo term (18) yields

$$\begin{aligned} \xi_{\mu}^{2h}(\theta) &\approx 4 \int_0^{\infty} d\chi W^2(\chi) d_A^{-2}(\chi) \\ &\times \left[ \int dM b(M)n(M) \frac{M}{\rho_0} \right]^2 \\ &\times \int \frac{ldl}{2\pi} P^L \left( k = \frac{l}{d_A(\chi)}; \chi \right) J_0(l\theta) \\ &= 4\xi_{\kappa}^{2h}(\theta). \end{aligned} \quad (20)$$

The 2-halo term (18) thus coincides with four times the 2-halo term of the convergence 2PCF in the weak lensing limit, as expected. However, the important point of the 2-halo term (18) is that it can correctly account for the contribution of non-linear magnifications ( $\mu \gtrsim 2$ ) on large scales.

Replacing  $P^{2h}(k)$  in equation (20) with a model of the non-linear mass power spectrum leads to the conventional method for predicting  $4\xi_{\kappa}(\theta)$  as an estimator of  $\xi_{\mu}(\theta)$ , as employed in the literature (e.g., Dolag & Bartelmann 1997; Sanz et al. 1997; Jain et al. 2003).

#### 4 ASYMPTOTIC BEHAVIOR OF MAGNIFICATION STATISTICS FOR HIGH MAGNIFICATIONS

Before proceeding with a detailed model prediction, let us demonstrate an intriguing property for the magnification statistics, its asymptotic dependence on high magnification events ( $\mu \gg 2$ ).

We restrict our discussion to point-like sources for simplicity, and we will later discuss about this. High magnifications ( $\mu \gg 2$ ) arise from images in the vicinity of the critical curve that is caused by an intervening mass concentration, such as halos. For any finite lens mass distribution, the critical curve must form a closed non-self-intersecting loop. Based on the catastrophe theory, it was shown in Blandford & Narayan (1986; also see Chapter 6 in Schneider et al. 1992) that the magnification of an image at a perpendicular distance  $\Delta\theta$  from the (fold) critical curve scales asymptotically as

$$\mu \propto \frac{1}{\Delta\theta}. \quad (21)$$

This argument holds independently of details of the lensing mass distribution, although the proportional coefficient does depend on the mass distribution.

To keep generality of our discussion, let us consider a correlation function between the magnification field and some cosmic fields expressed as

$$\xi(\theta; p) = \langle [\mu(\theta_1)]^p f(\theta_2) \rangle_{|\theta_1 - \theta_2| = \theta}, \quad (22)$$

where  $p$  is an arbitrary number. The field  $f$  is allowed to be constituted from any cosmic fields which are correlated with the magnification field. Therefore, the following argument holds for high-order moments beyond the two-point statistics if one takes products of the cosmic fields for  $f$ , e.g.  $f = \delta(\theta_2)\delta(\theta_3)$ .

Suppose that an intervening halo provides the critical curve in the lens plane for a given source redshift, as this is the case for an

NFW halo (see Figure 1). Then, let us consider how high magnifications in the vicinity of this critical curve contribute to the magnification statistics. By introducing an upper bound on the magnification fields as  $\mu \leq \mu_{\max}$ , we can address how the magnification statistics depends on the cutoff  $\mu_{\max}$  and what is the asymptotic behavior for the limiting case  $\mu_{\max} \rightarrow \infty$ . From equation (21), the cutoff  $\mu_{\max}$  corresponds to a lower limit on the perpendicular distance from the critical curve, say  $\Delta\theta \geq \epsilon$  ( $\epsilon \rightarrow 0$  corresponds to  $\mu_{\max} \rightarrow \infty$ ). As can be seen from equations (16) and (18), a picture of the halo model leads us to compute the high magnification contribution to the magnification statistics (22) by the integration

$$\xi(\theta; p, \mu_{\max}) \sim \int_{\partial S_c, \mu \leq \mu_{\max}} d^2s \frac{1}{|\Delta s|^p} f(|s + \theta|), \quad (23)$$

where  $\Delta s$  is the perpendicular distance from the critical curve and the integration range is confined to the area  $\partial S_c$  subject to the condition  $\mu \leq \mu_{\max}$ . The integration (23) results in one-dimensional integration for high magnifications around the critical curve, in analogy with equation (5.16) in Blandford & Narayan (1986) to derive the asymptotic, integral cross section for the strong lensing events that produce multiple images<sup>7</sup>. Hence, the leading order contribution of  $\mu_{\max}$  can be expressed as

$$\xi(\theta; p, \mu_{\max}) \sim \begin{cases} 1/\mu_{\max}^{1-p}, & p < 1 \\ \ln(\mu_{\max}), & p = 1 \\ \mu_{\max}^{p-1}, & p > 1. \end{cases} \quad (24)$$

where we have assumed that variation in the field  $f$  does not largely change for the relevant integration range. The equation above leads to an intriguing consequence: the amplitude of the magnification correlation is finite for  $p < 1$  for the limiting case  $\mu_{\max} \rightarrow \infty$ , while it diverges for  $p \geq 1$ . Furthermore, the asymptotic behavior does not explicitly depend on the separation angle  $\theta$  and therefore it holds even for large  $\theta$ . This means that the divergence  $\xi \rightarrow \infty$  for  $p \geq 1$  occurs even on degree scales, which is opposed to a naive expectation that the weak lensing approximation is safely valid on these scales. It is also worth stressing that this behavior is expected to hold for any lensing mass distribution once the critical curve appears, although the proportionality coefficient of  $\xi$  should depend on details of the mass distribution. These will be quantitatively tested by the halo model prediction as well as by the ray-tracing simulation.

In reality, a finite source size imposes a maximum cutoff on the observed magnification and thus the infinite magnification does not happen, even if a source sits on the caustic curve in the source plane (see Chapters 6 and 7 in Schneider et al. 1992; Peacock 1982; Blandford & Narayan 1996). For example, if the source is a circular disk with radius  $r_S$  and uniform surface brightness, the maximum magnification is given by  $\mu_{\max} \propto 1/\sqrt{r_S}$ . Therefore, to develop an accurate model prediction requires a knowledge of unlensed source properties in addition to modeling the lensing mass distribution. In particular, this could be crucial if one considers the magnification statistics (22) with  $p \geq 1$ , since it is very sensitive to large magnification events.

<sup>7</sup> The discussion in this paper as well as in Blandford & Narayan (1986) employs the assumption that asymptotic dependence of the magnification statistics on high magnifications is mainly due to images around the fold caustics and therefore ignores the contribution from the cusp caustic. This is likely to be a good approximation as shown in Mao (1992).

## 5 RESULTS

### 5.1 Ray-tracing simulations

To test the analytic method developed in §3, we employ the ray-tracing simulations. We will use the simulation for the current concordance  $\Lambda$ CDM model with  $\Omega_{m0} = 0.3$ ,  $\Omega_{\lambda0} = 0.7$ ,  $\Omega_{b0} = 0.04$ ,  $h = 0.7$  and  $\sigma_8 = 0.9$  (Ménard et al. 2002; Hamana et al. 2003; TJ03c). The  $N$ -body simulations were carried out by the Virgo Consortium<sup>8</sup> (see also Yoshida, Sheth & Diaferio 2001), and were run using the particle-particle/particle-mesh (P<sup>3</sup>M) code with a force softening length of  $l_{\text{soft}} \sim 30h^{-1}$  kpc. The initial matter power spectrum was computed using CMBFAST (Seljak & Zaldarriaga 1996). For the analytic model, we approximate the initial condition to use the CDM transfer function given by Bardeen et al. (1986) with the shape parameter in Sugiyama (1995) for simplicity. The  $N$ -body simulation employs  $512^3$  CDM particles in a cubic box of  $479h^{-1}$  Mpc on a side, and the particle mass of the simulation is  $m_{\text{part}} = 6.8 \times 10^{10}h^{-1}M_{\odot}$ .

The multiple-lens plane algorithm to simulate the lensing maps from the  $N$ -body simulations is detailed in Jain et al. (2000) and Hamana & Mellier (2001). We will use the output data for source redshifts of  $z_s = 1$  and 3 for the following analysis. The simulated map is given on  $1024^2$  grids of a size of  $\theta_{\text{grid}} = 0.2$ ; the area is  $\Omega_s = 11.7$  degree<sup>2</sup>. The angular resolution that is unlikely affected by the discreteness of the  $N$ -body simulation is around  $1'$  (Ménard et al. 2002; TJ03c).

### 5.2 Probability distribution function of the magnification: the angular resolution of the simulations

Universal properties of the critical curve, as demonstrated in §4, lead to an asymptotic behavior of the probability distribution function (PDF) of large magnification events, irrespective of details of the lensing mass distribution:  $\text{PDF}(\mu) \propto \mu^{-3}$  (Peacock 1982; Vierti & Ostriker 1983; Blandford & Narayan 1986; Schneider 1987; Hamana, Martel & Futamase 2000, and also see Chapters 6, 11 and 12 of Schneider et al. 1992). We use this property to investigate the angular resolution of the ray-tracing simulation we employ.

Figures 2 shows the magnification PDF measured in the simulations for source redshifts of  $z_s = 1$  and 3, respectively. To compute the PDF, we accumulate the counts in a given bin of  $\mu$  from 36 realizations and then normalize the PDF amplitude to satisfy  $\int d\mu \text{PDF}(\mu) = 1$  over the range of  $\mu$  measured. The PDF has a skewed distribution: most events lie in demagnification of  $\mu < 1$  and rare events have high magnifications with  $\mu \gg 2$  having a long tail. These reflect an asymmetric mass distribution in the large-scale structure as expected from the CDM scenario – the underdense region can be seen preferentially in the void region with a typical size  $\sim 10$  Mpc, while the highly non-linear structures appear in dark matter halos on scales  $\lesssim$  Mpc. As can be seen, the simulation of  $z_s = 3$  displays more pronounced evidence of asymptotic dependence  $\text{PDF}(\mu) \propto \mu^{-3}$  for high magnifications than the result for  $z_s = 1$ .

To more explicitly clarify the resolution issue of the simulations, we show the two results of the different smoothing scales that were used in making the projected density field to suppress the

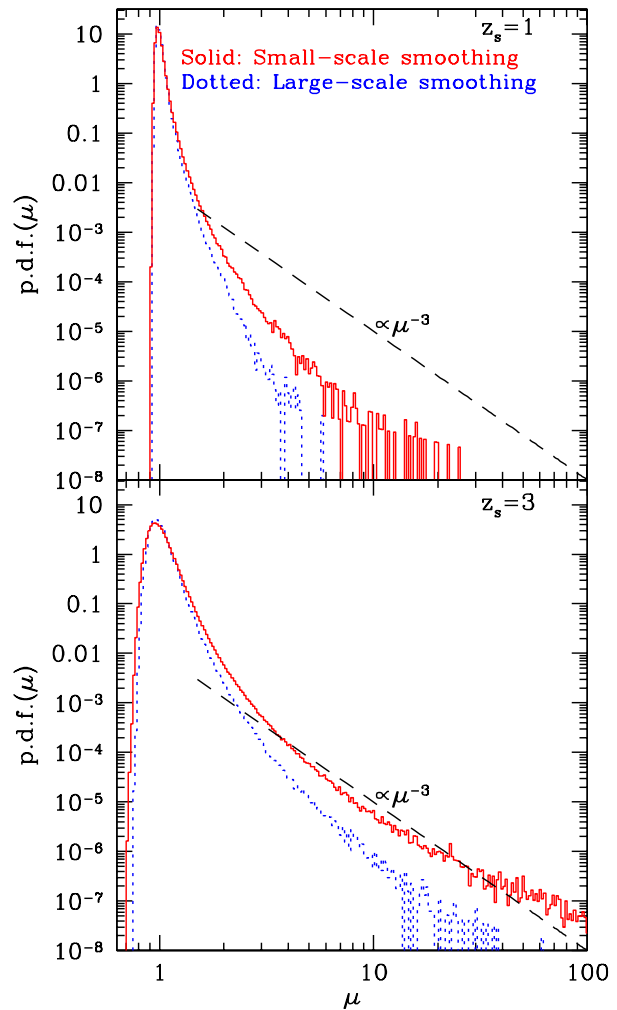


**Figure 2.** The probability density function (PDF) of the magnification measured from the ray-tracing simulations for  $z_s = 1$  and 3. To clarify the angular resolution, we show the two results of using different smoothing scales, which were used to avoid the artificial discrete effect of the  $N$ -body simulations. The comparison manifests that high magnification events are sensitive to smaller structures that are relevant for the smoothing scale. The dashed line shows an asymptotic behavior of the PDF for high magnification events,  $\text{PDF} \propto \mu^{-3}$ , as theoretically expected (see text in more detail).

discreteness effect of the  $N$ -body simulations (see Ménard et al. 2002 and Hamana et al. 2003 for more details). They are named as ‘small-scale smoothing’ (solid curve) and ‘large-scale smoothing’ (dotted curve), respectively. The former is expected to have the angular resolution around  $1'$  as discussed in Ménard et al. (2002) and in TJ03c, while the latter employs a smoothing scale two times larger than the former. The effect of the large-scale smoothing is that it more smoothes out smaller scale structures of the mass distribution that are resolved by the small-scale smoothing simulation. The comparison manifests that occurrence of high magnification events ( $\mu > 1$ ) is very sensitive to the small-scale structures. For this reason, we will employ the small-smoothing simulation in what follows. This result also implies that simulations with higher resolution could further alter the PDF shape especially at high magnification tail.

<sup>8</sup> see

<http://star-www.dur.ac.uk/~frazerp/virgo/virgo.html> for the details

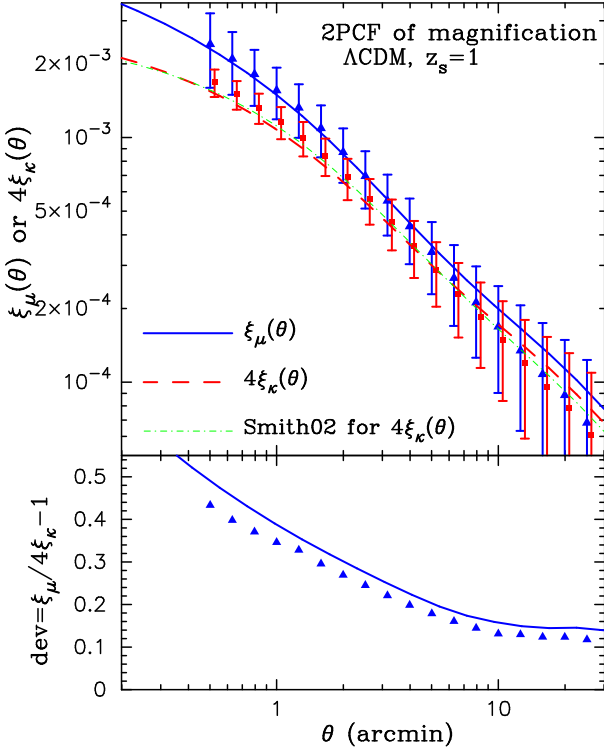


**Figure 3.** The two-point correlation function of the magnification field against the separation angle for the  $\Lambda$ CDM model and source redshift  $z_s = 1$ . For the halo model calculation, we employ the maximum magnification cutoff  $\mu_{\max} = 100$  (see text for the details). The solid curve shows the halo model prediction, while the triangle symbol is the simulation result. The error bar denotes the sampling variance for a simulated area of 11.7 degree<sup>2</sup>. For comparison, the weak lensing predictions, leading to  $\xi_\mu \approx 4\langle\kappa\kappa\rangle$ , are shown by the halo model (dashed curve), the simulation (square symbol) and the fitting formula of Smith et al. (2002; dot-dashed curve). Note that the simulation result is slightly shifted in the horizontal direction for illustrative purpose. The lower panel plots the contribution of non-linear magnifications,  $\xi_\mu/4\xi_\kappa - 1$ , for the halo model prediction and the simulation result.

### 5.3 The two-point correlation function of the magnification field

We now turn to investigation of the magnification 2PCF,  $\xi_\mu \equiv \langle \delta\mu \cdot \delta\mu \rangle$ . Figures 3 shows the comparison of the halo model prediction (solid curve) with the measurement from simulations (triangle symbol) for source redshift  $z_s = 1$ . Note that the error bar in each bin shows the sampling variance for a simulated area of 11.7 degree<sup>2</sup>, which is computed from 36 realizations. The errors in neighboring bins are highly correlated. For the halo model computation, we have used the magnification cutoff  $\mu_{\max} = 100$  – the 1- and 2-halo terms are calculated subject to the condition  $\mu_M \leq \mu_{\max}$  (see equations (16) and (18)). If we use  $\mu_{\max} = 30$ , the maximum value likely resolved by the simulation (see Figure 2), it reduces the amplitude of the halo model prediction only by  $\lesssim 10\%$  over the angular scales we consider. On the other hand, the mean value from the simulation realizations well converges for  $\mu_{\max} \gtrsim 10$  at level  $\lesssim 6\%$ , although the root-mean-square scatter among the realizations becomes larger by 20% at  $\sim 1'$  with increasing  $\mu_{\max}$ . This is because the presence of very high magnification events in some realizations largely enhances the magnifi-

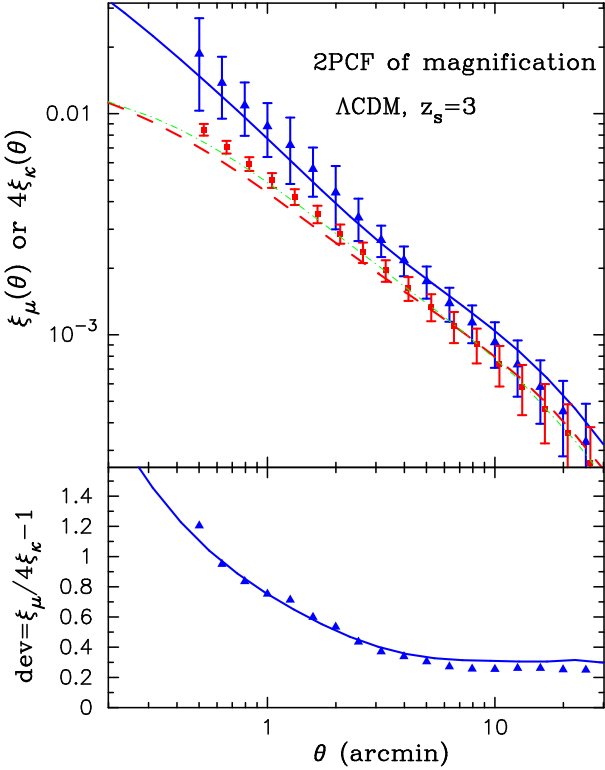


**Figure 4.** As in the previous figure, but for  $z_s = 3$ . For higher source redshifts, the non-linear magnification effect becomes more important as expected. The simulation result for  $\xi_\mu$  has larger sampling error than that for  $4\xi_\kappa$  due to the presence of high magnifications.

cation correlation function measured, and thus the scatter becomes large.

As can be seen, the halo model prediction well matches the simulation result. The 1-halo term provides dominant contribution to the total power on small scales  $\lesssim 3'$ , while the 2-halo term eventually captures the larger scale signal (see Figure A1 of TJ03c). It is worth noting that the shear field in  $\mu$  (see equation (1)) contributes to the 2PCF amplitude by  $\sim 10\%$  over the scales considered. To make clear the importance of the non-linear magnification contribution ( $\mu \gtrsim 2$ ), the dashed curve and the square symbol are the halo model prediction and the simulation result, respectively, when we employ the weak lensing approximation  $\mu \approx 1 + 2\kappa$ , leading to  $\xi_\mu \approx 4\langle\kappa\kappa\rangle = 4\xi_\kappa$ . For this case,  $4\xi_\kappa$  can be also computed from the fitting formula of the non-linear mass power spectrum recently proposed by Smith et al. (2002; hereafter Smith02), which demonstrates another test of the accuracy of the halo model as well as the simulation.

The lower panel explicitly plots the relative difference,  $\xi_\mu/4\xi_\kappa - 1$ , for the halo model and the simulation. The simulation result is computed from the mean values of  $\xi_\mu$  and  $4\xi_\kappa$ , and we do not plot the large error bar for illustrative simplicity. The non-linear magnification contribution amounts to  $\gtrsim 30\%$  at  $\theta \lesssim 2'$ , and the non-negligible contribution of  $\sim 10\%$  still remains even on large scales  $\gtrsim 10'$ . This is surprising, since it is naively expected that the weak lensing approximation is valid at these large scales. Our model of the 2-halo term (18) properly captures the non-linear effect seen in the simulation, although there are relatively large sampling variances on these scales. Ménard et al. (2002) also showed

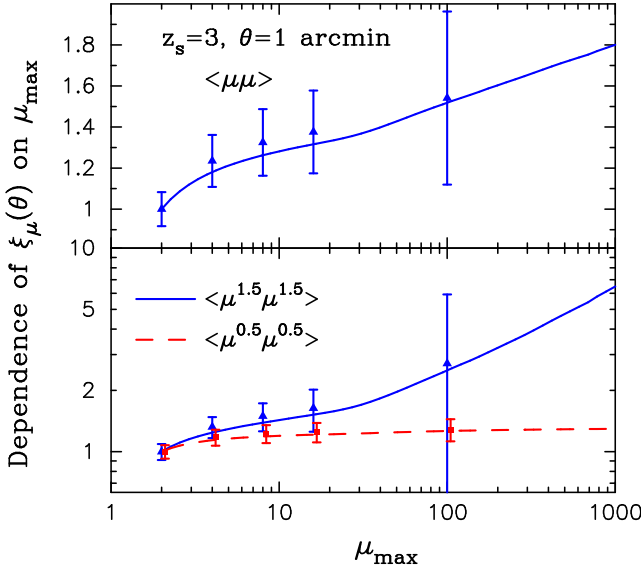


**Figure 5.** The dependences of the magnification 2PCF on the maximum cutoff used in the calculation. For the magnification correlation parameterized as  $\langle \delta\mu^p \cdot \delta\mu^p \rangle$ , the upper and lower panels show the results for  $p = 1$  and for  $p = 0.5$  and  $1.5$ , respectively. We consider  $z_s = 3$  and  $\theta = 1'$  for the source redshift and the separation angle, respectively. All the curves are normalized by their amplitude of  $\mu_{\max} = 2$ . As discussed in §4, it is expected that the 2PCF amplitude diverges for  $p \geq 1$  for the limiting case  $\mu_{\max} \rightarrow \infty$  (for point-like sources), while it is finite for  $p < 1$  (see equation (24)). This is verified by the halo model as well as by the simulation.

that the non-linear effect on the large scales can be fairly explained taking into account the higher-order terms  $O(\kappa^2)$  of the Taylor expansion of  $\mu$ , whereas the method ceases to be accurate on small scales  $\lesssim 5'$ . However, the important point we stress is that the perturbative treatment is likely to again break down on the large scales if we have an ideal simulation with sufficiently high angular resolution and as long as we ignore a source size effect (see also §4). On the other hand, one advantage of the halo model is that it allows us to explicitly introduce the maximum magnification cutoff in the calculation, by which a fair comparison with the simulation is allowed.

Figure 4 shows the result for  $z_s = 3$ , as in the previous figure. We again employed the maximum magnification cutoff  $\mu_{\max} = 100$  in the halo model calculation and the simulation result. If we use all the magnification events in the simulation, the mean value in each bin becomes largely noisy over a range of the angular scales, due to the presence of events with  $\mu > 100$  as shown in Figure 2. The high magnifications also cause large statistical scatters in each bin, as can be in part seen from the comparison of the simulation results for  $\xi_\mu$  and  $4\xi_\kappa$ . From the lower panel, it is clear that the non-linear magnification provides substantial enhancement of  $\gtrsim 50\%$  at  $\theta \lesssim 2'$  relative to the weak lensing prediction. The comparison with the previous figure manifests that sources at higher redshifts are more affected by the non-linear magnification, as the sources have more chance to encounter intervening halos.

#### 5.4 A quantitative test of the asymptotic behavior of the magnification statistics

In what follows we quantitatively and qualitatively test the asymptotic dependence of the magnification statistics on large magnifications ( $\mu \gg 2$ ), as derived in §4. For this purpose, we consider three cases of  $p = 0.5, 1.0$  and  $1.5$  for the magnification 2PCF parameterized as  $\xi = \langle \delta\mu^p \cdot \delta\mu^p \rangle$ , with source redshift  $z_s = 3$ . Figure 5 shows how the 2PCF amplitude depends on the magnification cutoff  $\mu_{\max}$  used in the halo model predictions and the simulation result. We consider  $\theta = 1'$  for the separation angle and the halo model prediction and the simulation result are normalized by their values at  $\mu_{\max} = 2$ . Note that  $\theta = 1'$  is chosen based on the fact that the scale is in the strongly non-linear regime and unlikely affected by the angular resolution of the simulation (TJ03c). The consequence of §4 is that the 2PCF amplitudes for  $p = 0.5, 1.0$  and  $1.5$  have the dependences on  $\mu_{\max}$  given as  $\xi \propto \mu_{\max}^{-0.5}, \ln(\mu_{\max})$  and  $\mu_{\max}^{0.5}$  for  $\mu_{\max} \gg 2$ , respectively. It is obvious that this consequence is verified by the halo model prediction and the simulation result for  $\mu_{\max} \gtrsim 10$ . Although the halo model results for  $p = 1.0$  and  $1.5$  display a bend at  $\mu_{\max} \approx 30$ , this is due to high magnifications between the radial and tangential critical curves in NFW halos. Most importantly, the 2PCF amplitude for  $p = 0.5$  has a well converged value for  $\mu_{\max} \gtrsim 5$ : the amplitude changes by less than 10% over  $\mu_{\max} = [10, 1000]$ . Therefore, the statistics with  $p < 1$  has a practically great advantage that it is little affected by the uncertainty in modeling the maximum magnification cutoff.

Finally, we note that the results shown above are unchanged even if we consider the cross-correlation  $\langle \delta\mu^p \cdot \delta^2 D \rangle$ , where  $\delta^2 D$  is the projected density fluctuation field (e.g., see equation (25)), because the asymptotic behavior is determined by the power of  $\mu$  entering into the general correlation function  $\langle \mu^p f \rangle$ , as derived in §4.

#### 5.5 Application to QSO-galaxy cross correlation

In this subsection, we consider an application of the halo model to the QSO-galaxy cross correlation. The angular fluctuation field of galaxies on the sky is a projection of the 3D galaxy fluctuation field  $\delta^g$  along the line-of-sight, weighted with the redshift selection function  $f_g(z)$  of the galaxy sample:

$$\delta n^g(\bar{\theta}) = \int_0^\infty dz f_g(z) \delta^g(d_A(z)\theta, z), \quad (25)$$

where  $f_g(z)$  is normalized as  $\int_0^\infty dz f_g(z) = 1$ . Throughout this paper, we employ

$$f_g(z)dz = \frac{\beta z^2}{z_0^3 \Gamma(3/\beta)} \exp \left[ -\left( \frac{z}{z_0} \right)^\beta \right] dz, \quad (26)$$

with  $\beta = 1.5$  and  $z_0 = 0.3$ . This model leads to the mean redshift as  $z_{\text{mean}} = \int dz z f_g(z) = 0.45$ .

However, a theoretical model of the galaxy fluctuation field  $\delta^g$  is not straightforward, since the galaxy formation is affected by complex astrophysical processes in addition to the gravitational effect. Recently, Jain et al. (2003) developed a sophisticated description of the magnification induced correlations based on the halo model as well as the galaxy semi-analytic model. In particular, it was shown that it is crucial to account for a model to describe how galaxies populate their parent halo, the so-called halo occupation number, to make accurate model predictions on arcminute angular scales. The halo occupation number largely depends on details of the galaxy sample taken (apparent magnitude range and so on) and

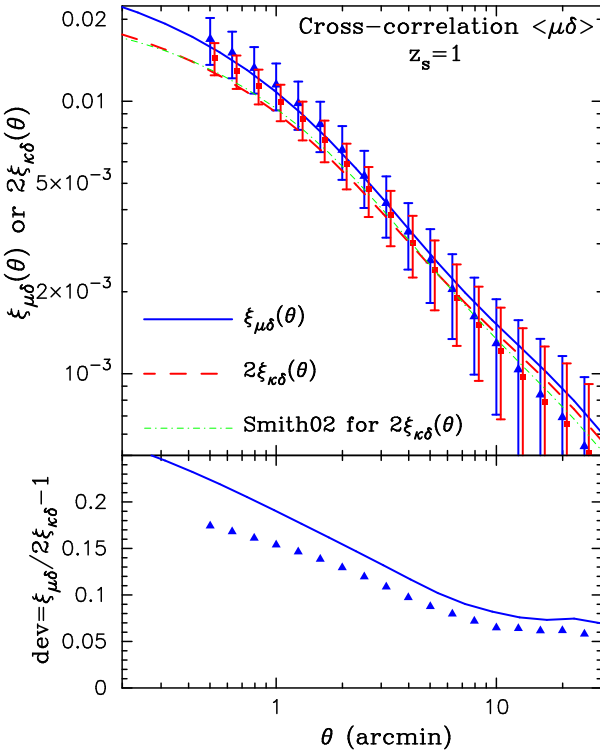


**Figure 6.** The cross correlation function between the magnification field and the projected density fluctuation field for  $z_s = 1$ , as in Figure 3. To get the projected density field, we assume the redshift selection function given by equation (26).

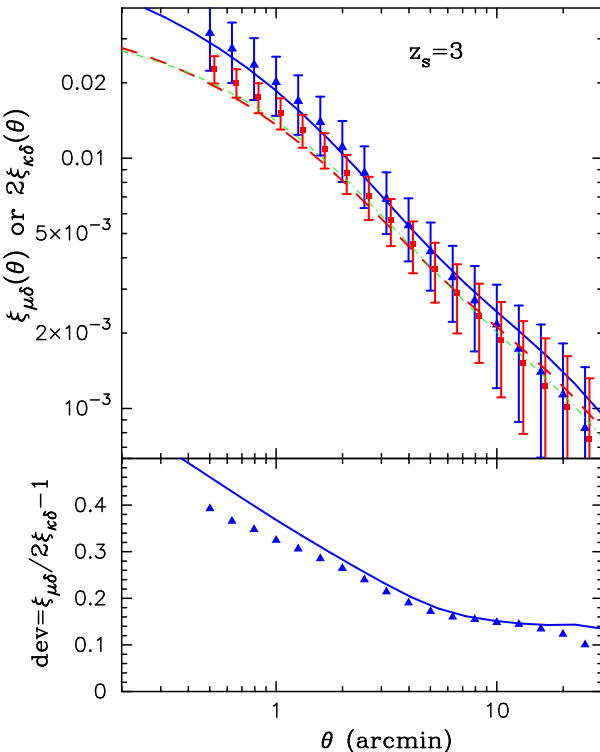


**Figure 7.** As in the previous figure, but for  $z_s = 3$ .

is sensitive to types of galaxies such red or blue galaxies. Our aim of this paper is to clarify the effect of the non-linear magnification. Therefore, rather than exploring the direction, we simply assume that the galaxy distribution exactly traces the underlying mass distribution;  $\delta^g = \delta$ . Extending the method presented in §3 leads to the 1-halo term contribution:

$$\xi_{\mu\delta}^{1h}(\theta) = \int_0^{\chi_H} d\chi \frac{d^2V}{d\chi d\Omega} f_g(z) \frac{dz}{d\chi} \int dM n(M) \frac{M}{\bar{\rho}_0} \times \int_0^\infty d\phi \int_0^{2\pi} d\varphi \phi [\mu_M^{2.5s-1}(\phi) - 1] \Sigma_M(|\phi + \theta|), \quad (27)$$

where  $\Sigma_M(x)$  is the normalized projected density of the NFW profile given by equation (26) in TJ03b. Similarly, one can derive the 2-halo term of  $\xi_{\mu\delta}$ , as done by equation (18).

Figures 6 and 7 show the results for source redshifts of  $z_s = 1$  and 3, respectively, as in Figures 3 and 4. Note that both the results employ the same redshift selection function (26) to obtain the projected density field. We simply assumed a special case of  $s = 4/5$  for the magnitude slope for the unlensed QSO number count. From the comparison with Figures 3 and 4, it is clear that non-linear magnification contribution is weakened, due to the single power of  $\mu$  entering into the two-point correlation compared to the magnification 2PCF. Nevertheless, it should be stressed that the non-linear effect has significant contribution of  $\gtrsim 15\%$  and  $\gtrsim 30\%$  at  $\theta \lesssim 1'$  for  $z_s = 1$  and 3, respectively, as can be explicitly seen in the lower panels.

## 5.6 Sensitivity of the magnification statistics to the halo profile properties

In this subsection, we address practically important questions: what can we learn from measurements of the magnification statistics? How is this method complementary to the established cosmic shear statistics that probes the correlations of the convergence or shear fields ( $\kappa$  or  $\gamma$ )? We demonstrate one example of this answer. The major difference between the magnification field  $\mu$  and the cosmic shear fields  $\kappa, \gamma$  is the non-linear effect of  $\mu$  (see equation (1)). The non-linear effect is more pronounced on smaller scales, as have so far been shown. Future massive surveys promise to measure the magnification statistics as well as the cosmic shear statistics even on sub-arcminute scales (Jain 2002; TJ03c; Jain et al. 2003). Within a picture of the halo model, the sub-arcminute correlation function is quite sensitive to the halo profile properties (TJ03b,c). Therefore, we here investigate the dependence of the magnification 2PCF on the halo profile parameters, the halo concentration and the inner slope of the generalized NFW profile. These parameters are still uncertain observationally and theoretically, and expected to have information on the dark matter nature as well as properties of highly non-linear gravitational clustering on  $\lesssim 1\text{Mpc}$ . Following TJ03c, we consider the parameterizations for the halo concentration and the halo profile given as  $c_0(M, z) = c_0(M/M_*)^{-0.13}$  and  $\rho(r) \propto r^{-\alpha} (1 + r/r_s)^{-3+\alpha}$ , respectively. Our fiducial model so far used is given by  $(c_0, \alpha) = (9.0, 1.0)$ . For cases  $\alpha = 0, 1$  and 2 we can derive analytic expressions for the convergence and shear profiles, which are necessary to compute the corresponding magnification profile (the expressions of the convergence fields are given in Appendix B in TJ03c). Note that in what follows we employ the virial boundary condition that makes it more straightforward to compute the halo model prediction for a general  $\alpha$ . The relevant angular scales are well below the reliable range that is not affected

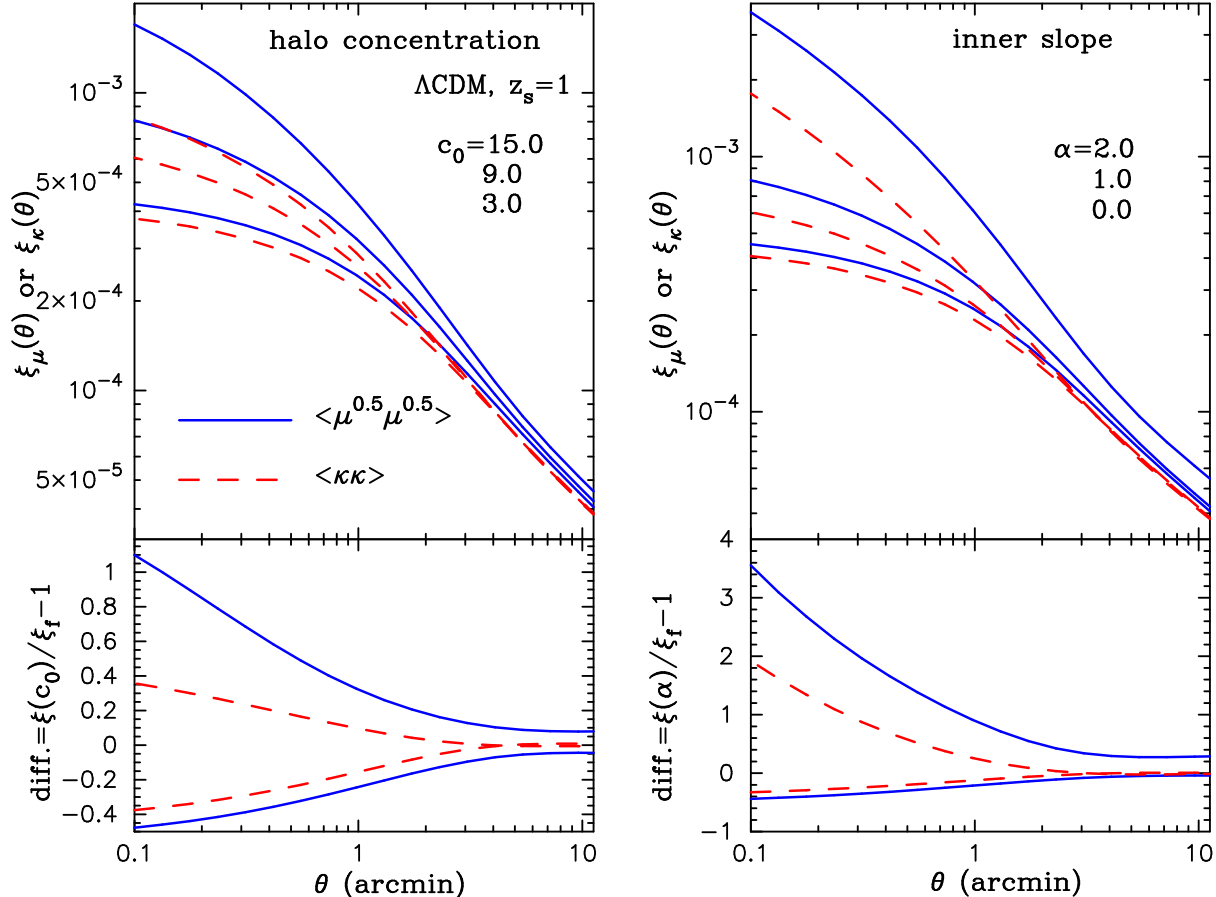


**Figure 8.** The dependences of the magnification 2PCF,  $\langle \delta\mu^{0.5} \cdot \delta\mu^{0.5} \rangle$ , on the halo profile parameters. The left panel shows the halo model predictions for the halo concentration parameter  $c_0 = 3, 9$  and  $15$  (from bottom to top), while the right panel shows the results with  $\alpha = 0, 1$  and  $2$  for the inner slope parameter of the generalized NFW profile (see text for more details). For comparison, the dashed curves are the corresponding results for the convergence 2PCF. Note that the magnification 2PCF considered becomes equivalent to the convergence 2PCF in the weak lensing limit as  $\delta\mu^{0.5} \approx \kappa$ . The lower panel shows the difference relative to the result with our fiducial model of  $\alpha = 1$  and  $c_0 = 9$ .

by the simulation resolution, and thus we will show the halo model prediction only.

The left panel of Figure 8 shows the halo model prediction for the magnification 2PCF with varying the halo concentration, while the right panel shows the results with varying  $\alpha$ . Here we consider  $\langle \delta\mu^{0.5} \cdot \delta\mu^{0.5} \rangle$  by the following two reasons. First is that it is less sensitive to high magnification events ( $\mu \gg 2$ ) and therefore observationally more robust. Second, it can be approximated by the convergence 2PCF (dashed curves), which is measured by the cosmic shear measurement, in the weak lensing limit because  $\delta\mu^{0.5} \approx \kappa$ . Therefore, the difference between the magnification and convergence correlations reflects contribution from mild non-linear magnifications. Halos with masses  $M \geq 10^{13} M_\odot$  provide dominant contribution of  $\gtrsim 80\%$  to the total power over a range of non-linear scales  $0.1\text{-}3'$  (e.g., see Figure 14 in TJ03c). One can see that the magnification 2PCF has stronger sensitivity to the halo profile parameters than the convergence 2PCF – increasing  $c_0$  or  $\alpha$  leads to substantial enhancement in the amplitude of the magnification 2PCF. This is because more concentrated profile with a fixed mass leads to greater critical radius and therefore it increases cross section of the non-linear magnifications to the correlation evaluation. In TJ03c, it was pointed out that the cosmic shear measurement introduces a degeneracy in determining these halo profile parameters,

even provided that we have an accurate measurement of the cosmic shear correlations down to sub-arcminute scales (see Figures 16 and 17 in TJ03c). The results in Figure 8 thus indicate that a joint measurement of the magnification statistics and the cosmic shear can be used to improve the parameter determinations. In particular, since the magnification correlation is more sensitive to higher  $\alpha$  and  $c_0$ , the measurement can put strong upper bounds on these parameters.

## 6 DISCUSSIONS

In this paper, we have used the real-space halo approach to compute the magnification correlation function without employing the weak lensing approximation  $\mu \approx 1 + 2\kappa + O(\kappa^2)$ . Our focus has been on the contribution of non-linear magnification ( $\mu \gtrsim 2$ ) to the correlation function that arises from lensing fields around halos. It has been shown that, even though halos are rare objects in the large-scale structure, they could have considerable impact on the magnification statistics. The encouraging result shown is the halo model prediction remarkably well reproduces the simulation result over the angular scales we consider (see Figures 3-7). The non-linear effect is more important as one considers the correlation function for

sources at higher redshifts and on smaller angular scales, where the weak lensing approximation ceases to be accurate. For example, the non-linear magnification induces a substantial enhancement in the 2PCF amplitude by  $\gtrsim 50\%$  at  $\theta \lesssim 3'$  relative to the weak lensing prediction (see Figure 4).

We find that the magnification statistics can be used to extract cosmological information complementary to that provided from the cosmic shear measurement. We have demonstrated that the joint measurement on angular scales  $\lesssim 3'$  can be used to precisely constrain the halo profile properties (see Figure 8). This possibility would open a new direction in using the magnification statistics as a cosmological probe beyond determination of fundamental cosmological parameters (Bartelmann 1995; Bartelmann & Schneider 2001; Ménard & Bartelmann 2002; Ménard et al. 2002). Exploring the halo profile properties with gravitational lensing will be a direct test of the CDM scenario in the highly non-linear regime  $\lesssim \text{Mpc}$ , since alternative scenarios have been proposed in order to reconcile the possible conflicts between the CDM predictions and the observations on the small scales (e.g., Spergel & Steinhardt 2000).

The results shown in this paper have important implications to actual measurements expected from forthcoming massive surveys. We derived an asymptotic behavior of the magnification correlation for large magnifications ( $\mu \gg 2$ ), from the universal lensing properties in the vicinity of critical curves (see §4). The intriguing consequence is that, for a correlation function parameterized as  $\langle \mu^p f \rangle$ , the amplitude converges to be finite for  $p < 1$  and otherwise diverges  $p \geq 1$  as  $\mu_{\text{max}} \rightarrow \infty$ , independent of details of the lensing mass distribution. This was quantitatively verified by the halo model prediction as well as by the simulations (see Figure 5). This result implies that, if we deal with the magnification statistics with  $p \geq 1$  that are sensitive to high magnifications, it is necessary to incorporate a modeling of the maximum magnification into the theoretical model, in order to make a correct interpretation of the measured signal. The maximum magnification is physically determined by the finite source size and the surface brightness distribution, which are not direct observable. We should thus care about additional uncertainty in the theoretical model, even if the halo model allows us to explicitly introduce the maximum magnification cut-off in the calculation. On the other hand, the promising result we stress is that, for the magnification correlation with  $p < 1$ , the amplitude is insensitive to high magnifications of  $\mu \gg 2$  (see Figure 5), which makes it more robust to compare the model prediction with the measurement. Nevertheless, the magnification correlation amplitude is significantly enhanced by modest non-linear magnifications of  $\mu \gtrsim 2$  relative to the weak lensing prediction (see Figure 8). This is the case for the two-point correlation of size (not area) fluctuations of distant galaxy images and for the QSO-galaxy cross correlation, if the unlensed number count of QSOs with a limiting magnitude has a slope of  $s = d \ln N(m)/dm < 4/5$ .

One might imagine that the non-linear magnification contribution can be suppressed by clipping regions of cluster of galaxies from survey data, e.g., as discussed in Barber & Taylor (2002). However, this could add artificial selection effect in the analysis. In addition, the lensing projection makes it relatively difficult to correctly identify the cluster region from the reconstructed convergence map, unless accurate photo- $z$  information or follow-up observations are available (e.g., White et al. 2002). The approach of this paper allows us to treat data more objectively. It is also interesting to address how the magnification statistics analysis can be improved by combining with the statistical study of strong lensing.

There are some effects we have so far ignored in the halo model calculation. Most important one is the asphericity of halo

profile in a statistical sense. The aspherical effect could lead to substantial enhancement of the magnification correlation amplitude, since it is known that an area enclosed by the critical curve is largely increased by ellipticity of the lensing mass distribution, thus increasing the cross section of high magnifications to the correlation evaluation. For example, the number of strong lensing arcs due to clusters of galaxies is amplified by an order of magnitudes if one considers an elliptical lens model instead of an axially symmetric profile (e.g., Meneghetti et al. 2003; Oguri et al. 2003). For the same reason, substructures within a halo could have strong impact on the magnification correlation, as they naturally emerges in the CDM simulations. Hence, it is of great interest to investigate these issues with higher resolution simulations.

Finally we comment on the QSO-galaxy cross correlation (see §5.5). Throughout this paper, we have ignored the galaxy biasing. In Jain et al. (2003) it was shown that it is of critical importance to take into account the non-linear biasing of galaxy clustering in modeling the cross correlation. The prediction on small scales  $\lesssim 10'$  is considerably sensitive to an input model of the halo occupation number. Therefore, incorporating the halo occupation number into the halo model method of this paper still remains to be examined. This study will be valuable in that massive surveys such as the SDSS and CFHT Legacy survey promise to measure the magnification effect with unprecedented accuracy.

We are grateful to Bhuvnesh Jain for collaborative work, valuable discussions and a careful reading of the manuscript. T. H. would like to thank for his warm hospitality at University of Pennsylvania, where a part of this work was done. M. T. also thanks Masamune Oguri for useful discussion. T.H. also acknowledges supports from Japan Society for Promotion of Science (JSPS) Research Fellowships. Numerical computations presented in this paper were partly carried out at ADAC (the Astronomical Data Analysis Center) of the National Astronomical Observatory, Japan.

## REFERENCES

Barber, A. J., Taylor, A. N., 2002, astro-ph/0212378  
 Bardeen, J. M., Bond, J. R., Kaiser, N., Szalay, A. S., 1986, ApJ, 304, 15  
 Bartelmann, M., 1995, A&A, 298, 661  
 Bartelmann, M., 1996, A&A, 313, 697  
 Bartelmann, M., Narayan, R., 1995, ApJ, 451, 60  
 Bartelmann, M., Schneider, P., 2001, Phys. Rep. 340, 291  
 Benítez, N., Martínez-González, E., 1997, ApJ, 477, 27  
 Benítez, N., Sanz, J. L., Martínez-González, E., 2001, MNRAS, 320, 241  
 Blandford, R. D., Narayan, R., 1986, ApJ, 310, 568  
 Blandford, R. D., Saust, A. B., Brainerd, T. G., Villumsen, J. V., 1991, MNRAS, 251, 600  
 Broadhurst, T. J., Taylor, A. N., Peacock, J. A., 1995, ApJ, 438, 49u  
 Bullock, J. S., Kolatt, T. S., Sigad, Y., Somerville, R. S., Kravtsov, A. V., Klypin, A. A., Primack, J. R., Dekel, A., 2001, MNRAS, 321, 559  
 Cooray, A., Sheth, R., 2002, Phys. Rep., 372, 1  
 Dolag, K., Bartelmann, M., 1997, MNRAS, 291, 446  
 Gaztañaga, E., 2002, astro-ph/0210311  
 Hamana, T., Mellier, Y., 2001, MNRAS, 327, 169  
 Hamana, T., Martel, H., Futamase, T., 2000, ApJ, 529, 56  
 Hamana, T., et al. 2002, astro-ph/0210450  
 Hamana, T., et al. 2003, in preparation  
 Hattori, M., Kneib, J.-P., Makino, N., 1999, Prog. Theor. Phys. Suppl., 133, 1  
 Hu, W., & Kravtsov, A., 2002, astro-ph/0203169  
 Jain, B., 2002, ApJ, 580, L3  
 Jain, B., Scranton, R., Sheth, R., 2003, astro-ph/0304203  
 Jain, B., Seljak, U., White, S. D. M., 2000, ApJ, 530, 547

Jarvis, M., Bernstein, G., Jain, B., Fischer, P., Smith, D., Tyson, J. A., Wittman, D., 2003, AJ, 125, 1014

Kaiser, N., 1992, ApJ, 388, 272

Mao, S., 1992, ApJ, 389, 63

Mellier, Y., 1999, ARAA, 37, 127

Ménard, B., Bartelmann, M., 2002, A&A, 386, 784

Ménard, B., Hamana, T., Bartelmann, M., Yoshida, N., 2002, astro-ph/0210112

Meneghetti, M., Bartelmann, M., Moscardini, L., 2003, MNRAS, 340, 105

Miralda-Escude, J., 1991, ApJ, 380, 1

Moessner, R., Jain, B., 1998, MNRAS, 294, L18

Navarro, J., Frenk, C., White, S. D. M., 1997, ApJ, 490, 493 (NFW)

Oguri, M., Lee, J., Suto, Y., 2003, submitted to ApJ

Peacock, J. A., 1982, MNRAS, 199, 987

Sanz, J. L., Martínez-González, E., & Benítez, N., 1997, MNRAS, 291, 418

Schneider, P., 1987, ApJ, 319, 9

Schendier, P., Weiß, A., 1986, A&A, 164, 237

Schneider, P., Ehlers, J., Falco, E. E., 1992, Gravitaional Lenses (Heidelberg: Springer)

Scoccimarro, R., Couchman, H. M. P., 2001, MNRAS, 325, 1312

Seljak, U., 2000, MNRAS, 318, 203

Seljak, U., Zaldarriaga, M., 1996, ApJ, 469, 437

Smith, R. E., Peacock, J. A., Jenkins, A., White, S. D. M., Frenk, C. S., Pearce, F. R., Thomas, P. A., Efstathiou, G., Couchman, H. M. P., 2002, astro-ph/0207664 (Smith02)

Sheth, R. K., Tormen, G., 1999, MNRAS, 308, 119

Spergel, D. N., Steinhardt, P. J., 2000, Phys. Rev. Lett., 84, 3760

Sugiyama, N., 1995, ApJ Suppl., 100, 281

Takada, M., Jain, B., 2002, MNRAS, 337, 875, astro-ph/0205055 (TJ02)

Takada, M., Jain, B., 2003a, ApJ, 583, L49, astro-ph/0210261 (TJ03a)

Takada, M., Jain, B., 2003b, MNRAS in press, astro-ph/0209167 (TJ03b)

Takada, M., Jain, B., 2003c, submitted to MNRAS, astro-ph/0304034 (TJ03c)

Vietri, M., Ostriker, J., 1983, ApJ, 267, 15

Yoshida, N., Sheth, R., Diaferio, A., 2001, MNRAS, 328, 669

Yoshida, N., Springel, V., White, S. D. M., Tormen, G., 2000, ApJ, 544, L87

Vale, C., White, M., 2003, astro-ph/0303555

Van Waerbeke, L., Hamana, T., Scoccimarro, R., Colombi, S., Bernardeau, F., 2001, MNRAS, 322, 918

Weinberg, S., 1978, ApJ, 208, L1

White, M., 2002, ApJ Suppl., 143, 241

White, M., Van Waerbeke, L., Mackey, J., 2002, ApJ, 575, 640

Zehavi, I., et al. 2003, submitted to ApJ, astro-ph/0301280